Solid State Phenomena
ISSN: 1662-9779, Vol. 387, pp 143-151
doi:10.4028/p-9qL9HL

Submitted: 2026-01-24
Revised: 2026-02-14
Accepted: 2026-02-17
Online: 2026-04-14

Iterative Un-Forming of Highly Aligned Discontinuous Preform/Material

Yuncong Feng[1,a*], Hao Yuan[1,b], Burak Ogun Yavuz[1,c], Ian Hamerton[1,d], Byung Chul Kim[1,e], Stephen R Hallett[1,f] and Jonathan P.-H. Belnoue[1,g]

[1]Bristol Composite Institute, University of Bristol, UK

[a]ol24008@bristol.ac.uk, [b]hao.yuan@bristol.ac.uk, [c]ogun.yavuz@bristol.ac.uk, [d]ian.hamerton@bristol.ac.uk, [e]B.C.Eric.Kim@bristol.ac.uk, [f]Stephen.Hallett@bristol.ac.uk, [g]jonathan.belnoue@bristol.ac.uk, (*corresponding author)

Keywords: Forming process, Finite Element Modelling, Automated Fibre Placement.

Abstract. Inherent limitations restrict the application of automated fibre placement (AFP) for manufacturing small components with complex geometries. As an alternative, flat, tailored preforms composed of fibre tows are first created and then formed into desired 3D geometries. However, the fibre orientation deviations between the as-manufactured and as-designed parts are inevitably introduced during forming. To address this issue, this study presents an iterative numerical forming/un-forming framework for the manufacture of highly aligned discontinuous preforms. At first, the as-designed preforms are "un-formed," i.e., a reverse forming simulation, to achieve the corresponding flat preforms using the finite element modelling (FEM) method. To mitigate the deviations during forming, a pre-compensation strategy is then introduced by adjusting the initial fibre orientations derived from the un-forming analysis based on the calculated deviations through iterative re-forming simulations. A hypo-viscoelastic constitutive model implemented through a user-defined material subroutine captures the rate-dependent and orthotropic behaviour of the preforms during un-forming and re-forming. The FEM simulation results demonstrate significant reductions in fibre orientation deviation of formed 3D preforms through the iterative forming/un-forming framework, validating its applicability to a discontinuous fibre material on complex geometries.

1. Introduction

Automated Fibre Placement (AFP) is an efficient technique for large-scale composite manufacturing with minimal human error. However, its application to small components remains limited due to the relatively large size of AFP heads and machines, as well as challenges in depositing fibres on small radii of curvature.

To address these limitations, our research group has proposed an alternative method that enables fast manufacturing of low-defect highly-optimised doubly curved parts. The approach starts with the creation of flat, tailored preforms composed of fibre tows, followed by forming onto the desired 3D geometry. Deviations between the as-manufactured and as-designed parts occur in the forming process due to shear deformation of tows. To mitigate these deviations, a virtual un-forming process is introduced, in which the as-designed 3D part is computationally un-formed into flat tailored preforms [5, 6]. The flat preform fibre paths extracted from the analyses are used to manufacture physical preform through the continuous tow shearing method [7].

Previous studies have modelled preforms with continuous fibres in the un-forming process [7]. However, with the growing emphasis on sustainability, discontinuous fibres are increasingly favoured because they can come from recycled material. Given the distinct mechanical behaviours of preforms reinforced with continuous and discontinuous fibres, the applicability of the un-forming approach requires verification for discontinuous-fibre systems. Moreover, in existing studies, the 2D fibre paths were obtained directly from the un-forming simulation, which is difficult to realise for complex geometries with sharp curvature variations, such as automotive parts.

In this study, highly aligned discontinuous fibre prepregs with a thermoset resin matrix are investigated [1, 2]. The preforms consisting of thermoset resin matrix, reinforced by highly aligned discontinuous fibres, are formed utilising the double diaphragm forming (DDF) technique. A user subroutine based on the HypoDrape Abaqus VUMAT, developed at BCI and introduced in Section

5, is employed to describe the behaviour of preforms during the forming and un-forming processes [3]. To enable general applicability to parts with complex geometries and viscoelastic behaviours not previously reported in the literature, an iterative forming–unforming design strategy is introduced to improve the accuracy of the existing unforming model, thereby supporting more robust composite manufacturing design.

2. Modelling and Automation Strategy

Figure 1 illustrates the workflow of forming/un-forming is depicted in. First, a DDF process is simulated on a "surrogate" preform to obtain the deformation history of the nodes of both diaphragms. This displacement history is then reversely applied to the diaphragms, with the surrogate preform replaced by preforms with realistic material properties, in the un-forming simulation. Subsequently, the resulting flat preforms are re-formed to verify if fibre paths in the formed part agree with those in the as-designed part. If the deviation in the fibre path exceeds a certain tolerance, corrected fibre orientations, determined through a pre-compensation algorithm, are then applied to the flat preforms before repeating the re-forming process. These procedures are repeated until the deviation falls within the specific tolerance. Finally, the corrected fibre paths from the un-forming simulation are obtained as the input for the future AFP manufacturing.

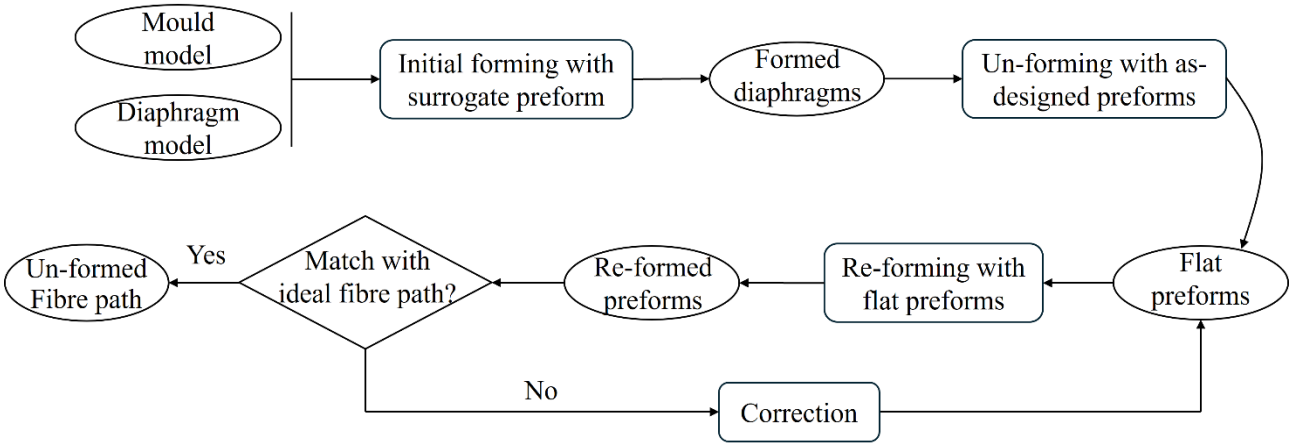

Fig. 1. The flowchart of forming and un-forming processes

In the forming/unforming workflow, key information, such as nodal displacements and fibre orientations, is exported from the Abaqus database, processed, and then re-imported into the Abaqus/Explicit solver for further analyses. The fibre orientation, in particular, requires these procedures to be repeated iteratively. Performing this process manually, step by step, is time-consuming; therefore, Python scripts were developed to automate and streamline the entire workflow, enabling one click execution. For the initial forming simulation, a Python script was used to export the nodal displacement histories of the diaphragms, along with the node and element information of the surrogate preform and formed diaphragms at the end of the simulation. The histories were then processed in reverse time and exported as include files containing the settings of boundary conditions and their corresponding amplitudes. These files were then incorporated into an input (.inp) file — also automatically generated by the script — for the un-forming simulation, which included the diaphragm and preform models and all relevant analysis settings. The script allowed the number of preforms to be specified, and the assembly module was adjusted accordingly to accommodate the defined configuration. Finally, the input file was submitted to Abaqus Explicit by the script. Afterwards, another Python script was created to export and correct fibre orientations from the un-forming analysis, and to generate an input file containing the corrected orientations for the re-forming simulations. At current, the correction requires manual intervention, but this will be fully automated in the future work.

3. Mould and Specimen Design

A revolving-swept and double-curved 3D surface was designed to demonstrate the advantages of the proposed forming/un-forming framework and to validate the overall workflow. A margin region with the length of 5 mm from the surface was introduced to mitigate the edge effects on preform deformation in the forming process. The 2D project of the overall geometry is a square with the length of 114.3 mm, as demonstrated in Figure 2(a). It should be noted that only the top surface of the virtual mould, i.e. the region that interacts with the preforms and diaphragms, was modelled, to simplify the creation of geometric model. The CAD geometry was built in CATIA V5 and then imported into Abaqus, where it was discretised into membrane elements with a rigid body assignment.

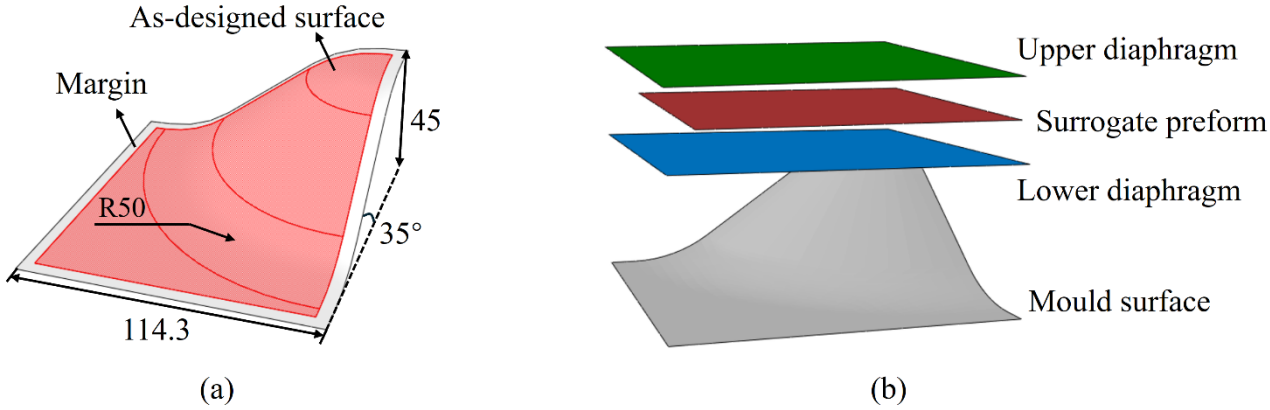

Fig.2. (a) Basic dimensions of the mould surface (units: mm). (b) Schematic of the DDF setup.

Typically, the 3D surface is imported into Abaqus again to serve as the specimen, after which a structural mesh is applied to align element profiles with fibre paths, therefore preventing potential numerical errors. However, as structural mesh follows the contour gradient of the geometry, the gradually converging gradient along the diagonal direction towards the corner of the specimen in this case leads to highly irregular element distributions. To tackle this issue, the structural mesh of the target 3D surface was instead obtained from a forming simulation on a "surrogate" preform, the details of which are provided in Section 4.

4. Initial Forming Simulation

The initial forming model consists of two diaphragms, a "surrogate" preform in between the diaphragms and the mould surface on the bottom, as shown in Figure 2(b). The edges of the diaphragms were constrained to move only in the vertical direction, while the mould surface was completely fixed. Atmospheric pressure was applied to the top diaphragm to form the double-diaphragm system. It should be noted that the purpose of the initial forming simulation was to extract the displacement histories of diaphragms for use in the subsequent un-forming simulation. Because the preform bending stiffness is negligible relative to diaphragm interaction forces [7]. its configuration does not meaningfully influence diaphragm deformation. The surrogate preform is used solely to provide mesh continuity; an isotropic model is therefore sufficient. Specifically, Young's modulus and Poisson's ratio were set to 160 MPa and 0.1, respectively, to increase the shear resistance and thereby reduce localised shear deformation. Bulk viscosity was added into the system to suppress element distortion. Friction is a crucial factor that affects the forming pattern of diaphragms and the preform. The penalty coefficients for frictions between diaphragm-diaphragm and diaphragm-preform were set to 0.6 and 0.53, respectively, based on the results of characterisation experiments reported in [8]. For the material model of diaphragms, Ogden's hyperelastic material model was adopted with the same parameters used in [3], which are listed in Table 1. The diaphragms and the preform were structurally meshed using S4R shell elements. The element thicknesses were 0.2 mm and 0.15 mm for the diaphragms and the preform, respectively, with uniform element sizes of 4.5 mm for the diaphragms and 2 mm for the preform. The element

size was selected with reference to [7]. The primary objective of this work is to develop and demonstrate the iterative forming/un-forming framework rather than to resolve local stress and strain fields. Moreover, as the displacement fields of both the preforms and diaphragms are smooth, further mesh refinement would not alter the conclusion of this work while significantly increasing computational cost. Consequently, mesh convergence analysis was not conducted in this study.

Table 1. Material parameters for Odgen's hyperelastic model for the diaphragms from [3].

Material parameters	μ_1(Pa)	a_1	μ_2(Pa)	a_2
Value	150,904	3.0918	813.392	0.81451

After forming, the preform with a uniform structural mesh was obtained, as shown in Figure 3(a) and (b), and was used as the discretised geometry model of the as-designed part for the un-forming simulation. In addition, the nodal displacement histories of both diaphragms were extracted and time-reversed to serve as prescribed boundary conditions for the diaphragms in the un-forming analysis.

5. Un-Forming and Re-Forming Simulations

In this study, two preform sheets, denoted as *Sheet0* and *Sheet1*, were un-formed as as-designed preforms. Both sheets used the meshed geometry of the preform obtained in the initial forming analysis, but their fibre directions were configured differently. In *Sheet0*, the fibre paths were aligned with element edges along the *x* axis, whereas in *Sheet1*, the fibre paths were oriented along the *y* axis, as illustrated in Figure 3 (a) and (b). Due to the viscoelastic nature of the thermoset resin, the mechanical response of the preform is strongly dependent on the deformation rate. Accordingly, an analytical viscoelastic constitutive model developed in our previous work [4] was employed to describe the behaviour of the preform in the un-forming and re-forming simulations. In addition, to capture the orthotropic characteristics of the preform accurately, its constitutive behaviour was implemented using a hypo-viscoelastic material model via a VUMAT subroutine in Abaqus/Explicit. To eliminate the effect of rigid-body rotation of fibres, which can be significant during un-forming and re-forming, on the stress update, the deformed fibre direction was first calculated using the current deformation gradient to construct a fibre-aligned work frame. The strain increment under the Green–Naghdi (GN) work frame, i.e. the default Abaqus VUMAT work frame, was converted to the fibre work frame, where the stress increments were computed according to the constitutive relations and then converted back to the GN work frame for the next increment.

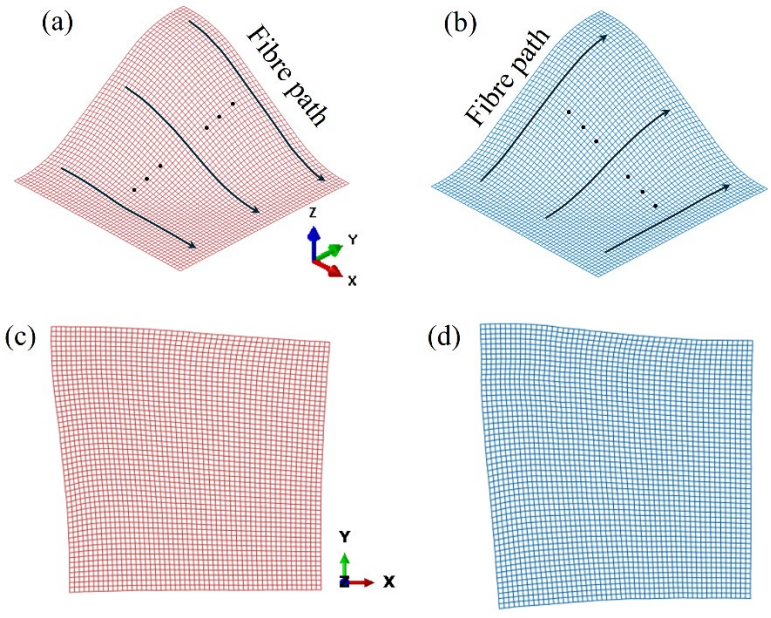

Fig. 3. (a) The as-designed 3D *Sheet0* and (b) the as-designed 3D *Sheet1*. (c) The un-formed 2D *Sheet0* and (d) the un-formed 2D *Sheet1*.

Due to the decoupling between the in-plane and out-of-plane behaviour of the preform, shell and membrane elements were utilised to simulate the collective material response of the preform sheets. In particular, shell elements (S4R in Abaqus/Explicit) accounted for out-of-plane bending, while in-plane deformation was evenly shared by both shell and membrane elements (M3D4R). Both element types were superimposed by sharing common nodes and assigned the same thickness, as described in Section 4. The material properties of the shell and membrane elements, obtained from characterisation experiments, are documented in Table 2. At the end of the un-forming simulation, the 3D sheets were reversely formed back into flat sheets, as demonstrated in Figure 3(c) and (d).

Table 2. Material input parameters for membrane and shell elements

Element type	E_1 (MPa)	E_2 (MPa)	G_{12} (MPa)
Membrane	Analytical model [4]	0.05	Analytical model [4]
Shell	Analytical model [4]	0.05	1×10^{-8}

To verify the un-forming results, the preforms were virtually re-formed and then compared with the as-designed preforms in terms of fibre orientation. To this end, the diaphragms and the flat preforms with updated fibre orientations from the un-forming analysis were input to the re-forming simulation as the initial state. Boundary conditions in the re-forming simulation remained the same with those in the initial forming simulation, while the surrogate preform was replaced by the un-formed 2D preforms with the viscoelastic material model applied. Afterwards, the fibre orientations of the re-formed 3D preforms were extracted for the calibration and correction of the deviation in fibre orientations.

6. Calibration and Correction of Fibre Orientation Deviations

The angular deviation between the fibre orientations of the as-designed and re-formed preforms was calculated and used as the basis for the subsequent correction. Its magnitude was obtained using the following equation:

$$|\Delta \boldsymbol{f}| = acos\left(\frac{\boldsymbol{f}_a \cdot \boldsymbol{f}_r}{|\boldsymbol{f}_a| \cdot |\boldsymbol{f}_r|}\right) \quad (1)$$

where $\boldsymbol{f}_a$ and $\boldsymbol{f}_r$ represent the fibre orientation vectors of the as-designed and re-formed preforms, respectively. acos is the inverse cosine function, and $\Delta \boldsymbol{f}$ denotes the angular deviation. In addition, the sign of the deviation is crucial for determining the direction of the correction. To this end, the 3D fibre vectors were projected onto a 2D plane, where $\boldsymbol{f}_a$ was transformed into a unit reference vector, i.e., (1,0) for *Sheet0* and (0,1) for *Sheet1*. The deviation was defined as positive when the component of $\boldsymbol{f}_r$ along the secondary axis was positive. In this case, the y and x axes served as the secondary axes for *Sheet0* and *Sheet1*, respectively. Python scripts were developed to visualise the angular deviation on the preforms to facilitate further verification. The deviation distributions after the re-forming process are demonstrated in Figure 4.

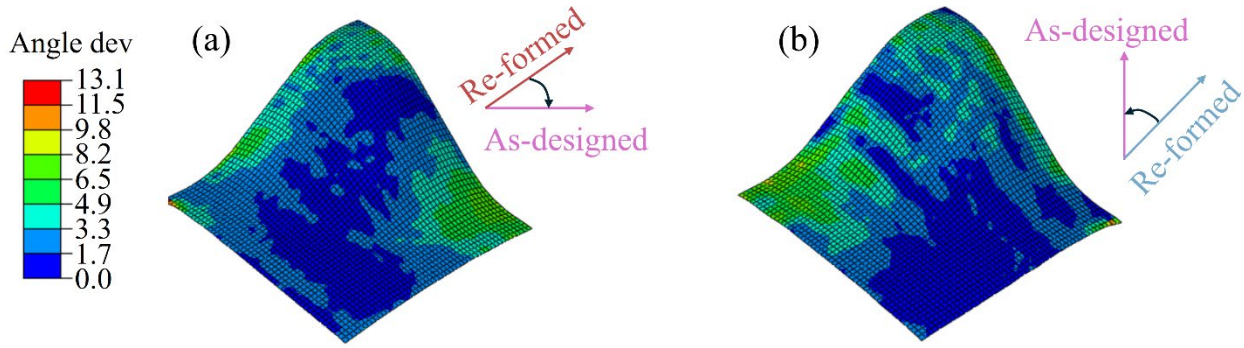

Fig. 4. The angular deviation distributions of (a) *Sheet0* and (b) *Sheet1* after the 1st re-forming simulation.

For the correction, the angular deviations obtained from the re-formed 3D preforms were inversely applied to the corresponding un-formed flat preforms, assuming that fibre reorientation during forming is systematic. To avoid over-correction, only a fraction of the deviation was pre-compensated in the initial fibre orientation of the flat preforms. The correction procedure is summarized as follows:

1. The initial angular deviation was calculated as the difference between the as-designed fibre orientation and the fibre orientation from the first re-formed preform simulation results.
2. A corrective rotation equal to $\alpha \times (-\Delta \boldsymbol{f})$ was applied to the initial fibre orientation of the flat preform, where α denotes the compensation factor.
3. The corrected flat preform was re-formed, and the resulting fibre orientation deviation was evaluated.
4. The value of α was updated according to a parametric optimisation method as described in the following five paragraphs.
5. Steps 2–4 were repeated until the minimum deviation was achieved.

Deviations on *Sheet0* and *Sheet1* were both positive, indicating that the re-formed orientations had different angular positions relative to the as-designed orientations in the two preforms, as illustrated in Figure 4. Therefore, opposite rotational pre-compensation was applied to the two preform sheets. In this study, anticlockwise compensation was defined as positive, and clockwise adjustment was defined as negative. To quantify the correction performance, the root mean squared error (RMSE) and a severity index were introduced, where the severity index represents the number of elements with the angular deviation exceeding half of the maximum deviation. As shown in Figure 4, the maximum deviation is 13.1°, and the corresponding severity threshold is therefore set to 6.55°. RMSE provides a global measure of the average magnitude of the angular deviation, while the half-maximum threshold prevents the severity index from becoming overly polarized by either isolated extreme values or a large population of minor deviations. A similar half-maximum–based thresholding strategy has been adopted in [9].

To identify the optimised α for each sheet, a commonly used approach is the bisection method [10], where α is halved repeatedly to ensure convergence toward the minimal deviation. However, as the number of compensation factors increases with the number of preform layers, the problem becomes multi-variable, rendering the bisection method less efficient. Therefore, a parametric optimisation strategy was adopted [11].

Initially, α = 1 and -1 were selected for *Sheet0* and *Sheet1*, respectively; however, both RMSE and the severity index of the corrected un-forming results exceeded those obtained without correction (RMSE = 4.41 and 4.12 for *Sheet0* and *Sheet1*, respectively; severity index = 279 and 218 for *Sheet0* and *Sheet1*, respectively), indicating overcorrection when the full angular deviation was applied to the un-forming analysis. Therefore, only a portion of the angular deviation was compensated. First, the α value for *Sheet1* was fixed at 0.1, while the α value for *Sheet0* was varied from 0.1 to the anticipated upper limit of 1.0 to investigate the influence of α value for *Sheet0* on angular deviation. It should be noted that the specific choice of α for *Sheet1* at this stage does not

affect the outcome. Due to the small bending of the preforms, the configuration of one preform has a negligible influence on the angular distribution of the other. This assumption is validated by the results shown in Figure 5 (a) and 5(b).

For *Sheet0*, a sharp increase in both RMSE and the severity index was observed when α exceeded 0.25, indicating that continuously increasing α beyond 0.4 is unnecessary. Consequently, the effective range of α for *Sheet0* was limited to 0.1–0.4. As illustrated in Figure 5 (a) and 5(b), the RMSE for *Sheet0* reaches a low-level plateau between α = 0.1 and 0.2, whereas the severity index remains stable up to α = 0.25. Based on these observations, α values of 0.1, 0.2, and 0.25 were selected for *Sheet0*. For each of these cases, α for *Sheet1* was varied from −0.1 to the anticipated lower limit of −1.0.

The results for α = 0.1 for *Sheet0* and α values ranging from −0.1 to −0.4 for *Sheet1* are presented in Figure 5 (c) and 5(d). Although RMSE continued to decrease with decreasing α for *Sheet1*, an increasing trend in the severity index was observed beyond α = −0.25. This result was deemed unacceptable, as it would be undesirable to permit a noticeable number of elements with large angular deviations, even if the majority exhibit only minor deviations. Therefore, the lower bound of α for *Sheet1* was set to −0.4.

Similar trends were observed when *Sheet0* was fixed at α = 0.2 and 0.25. However, the combination of α = 0.1 for *Sheet0* and α = −0.25 for *Sheet1* resulted in the smallest overall angular deviations. Accordingly, these values were selected as the optimal compensation factors, and the corresponding angular deviation distributions are presented in Figure 6.

Admittedly, the parametric approach cannot reduce all deviations to their absolute minimum. More localised optimisation strategies will therefore be explored in future work.

Compared to the 1st re-forming results, overall RMSE for *Sheet0* and *Sheet1* after final pre-compensation decreased by 6.5% and 15.8%, respectively. It should be noted that a large proportion of the preforms exhibited very small angular deviations (<1.7°). When focusing on the critical regions with relatively large deviations, the improvement in RMSE becomes considerably more pronounced. In addition, the number of severe elements was reduced by 43.2% and 221.9% for *Sheet0* and *Sheet1,* respectively. These results show that the effectiveness of the proposed forming/un-forming framework combined with the pre-compensation strategy.

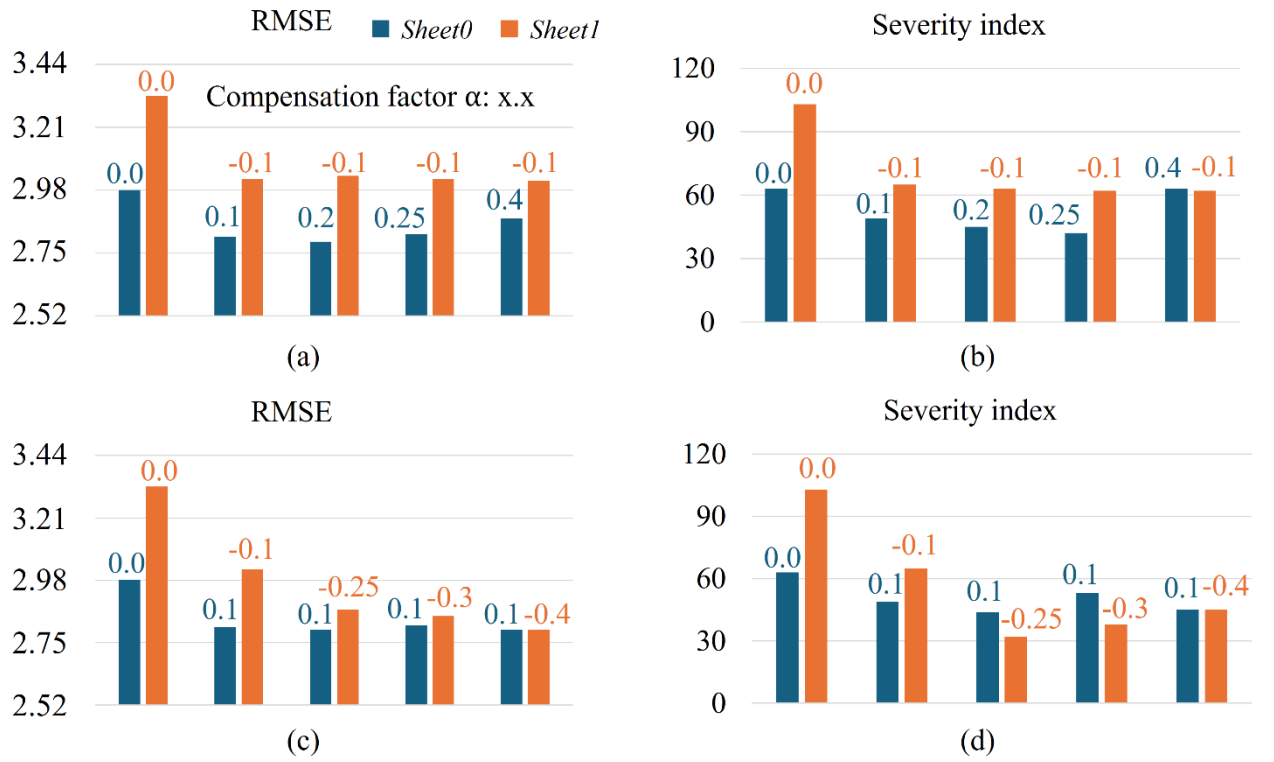

Fig. 5. (a) RMSE and (b) severity index for a set of re-forming simulation results with varying α for *Sheet0* and the constant α of 0.1 for *Sheet1*. (c) RMSE and (d) severity index for a set of re-forming simulation results with the constant α of 0.1 for *Sheet0* and varying α for *Sheet1*.

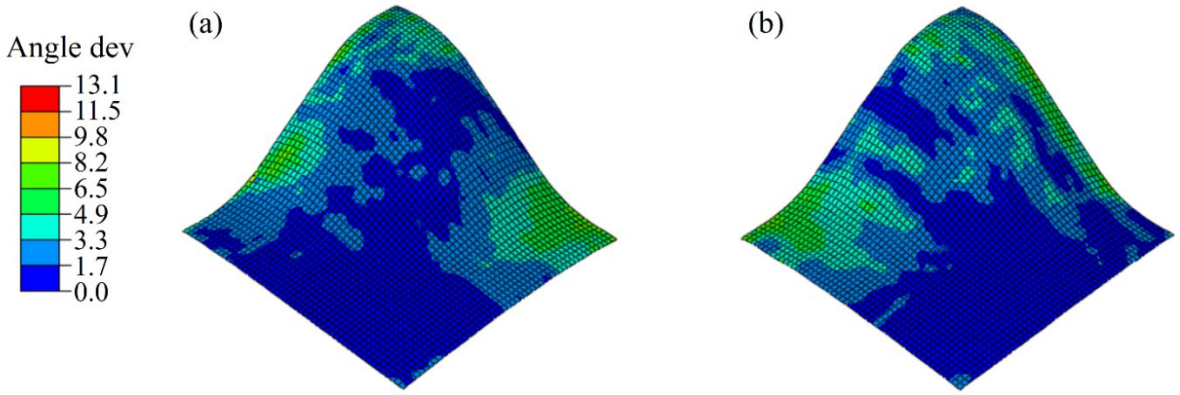

Fig. 6. Angular deviation distributions of (a) *Sheet0* and (b) *Sheet1* after final pre-compensation.

The parametric optimisation algorithm will be implemented as a Python script to determine the optimised automatically the compensation factor for each preform sheet. The resulting corrected fibre orientations will then be automatically converted into fibre paths for AFP manufacturing.

7. Conclusion

An iterative forming/un-forming framework was developed to improve the accuracy of un-forming simulations for discontinuous preforms, representing a clear improvement over direct un-forming analyses, particularly for complex geometries. A hypo-viscoelastic model was employed to accurately capture the preform behaviour during forming and un-forming. To mitigate the fibre orientation deviation introduced during forming, a pre-compensation strategy was introduced by optimising the compensation factor applied to the initial fibre orientations of the un-formed preforms through a parametric study. Comparative results before and after pre-compensation demonstrate a significant reduction in the angular deviation, confirming the effectiveness of the proposed iterative forming/un-forming framework.

References

[1] D. Heider, J. Tierney, M.A. Henchir, V. Gargitter, S. Yarlagadda, J.W. Gillespie Jr, J. Sun, J.M. Sietins, D. Knorr, Microstructural evaluation of aligned, short fiber Tuff material, SAMPE 2019-Charlotte, NC, May 2019 (2019).

[2] S. Yarlagadda, J. Deitzel, D. Heider, J. Tierney, J.W. Gillespie Jr, Tailorable universal feedstock for forming (TUFF): overview and performance, SAMPE 2019-Charlotte, NC, May 2019 (2019).

[3] A.J. Thompson, J.P. Belnoue, S.R. Hallett, Modelling defect formation in textiles during the double diaphragm forming process, Composites Part B: Engineering 202 (2020) 108357.

[4] B.O. Yavuz, I. Hamerton, M.L. Longana, J.P.H. Belnoue, Modelling the tensile behaviour of aligned discontinuous carbon fibre thermoplastic matrix composites under processing conditions, Composites Science and Technology 269 (2025) 111252.

[5] E. Loukaides, J. Allwood, Automatic design of sheet metal forming processes by "un-forming", International Journal of Mechanical Sciences 113 (2016) 61-70.

[6] J. Joustra, K. Brans, I. Fernandez Villegas, J. Sinke, J. Teuwen, Reverse forming thermoplastic composites: Design and process development, Composites Part C: Open Access 16 (2025) 100550.

[7] X. Sun, J.P.H. Belnoue, W.-T. Wang, B.C. Kim, S.R. Hallett, "Un-forming" fibre-steered preforms: Towards fast and reliable production of complex composites parts, Composites Science and Technology 216 (2021).

[8] S. Chen, O. McGregor, A. Endruweit, M. Elsmore, D. De Focatiis, L. Harper, N. Warrior, Double diaphragm forming simulation for complex composite structures, Composites Part A: Applied Science and Manufacturing 95 (2017) 346-358.

[9] R. Karim, P. Bhagirath, P. Claus, R.J. Housden, Z. Chen, Z. Karimaghaloo, H.-M. Sohn, L.L. Rodríguez, S. Vera, X. Albà, Evaluation of state-of-the-art segmentation algorithms for left ventricle infarct from late Gadolinium enhancement MR images, Medical image analysis 30 (2016) 95-107.

[10] R.M. Freund, The steepest descent algorithm for unconstrained optimization and a bisection line-search method, Journal of Massachusetts Institute of Technology. United States of america 131 (2004).

[11] R. Binali, A.D. Patange, M. Kuntoğlu, T. Mikolajczyk, E. Salur, Energy saving by parametric optimization and advanced lubri-cooling techniques in the machining of composites and superalloys: A systematic review, Energies 15(21) (2022) 8313.